Journal of Applied Physics

Surface passivation and aging of InGaAs/InP heterojunction phototransistors

Cite as: J. Appl. Phys. **121**, 233105 (2017); https://doi.org/10.1063/1.4986633
Submitted: 11 April 2017 . Accepted: 05 June 2017 . Published Online: 16 June 2017

Min-Su Park, Mohsen Razaei, Katie Barnhart, Chee Leong Tan, Hooman Mohseni, et al.

Surface passivation and aging of InGaAs/InP heterojunction phototransistors

Min-Su Park, Mohsen Razaei, Katie Barnhart, Chee Leong Tan, and Hooman Mohseni
Bio-inspired Sensors and Optoelectronics Laboratory (BISOL), Northwestern University, Evanston, Illinois 60208, USA

(Received 11 April 2017; accepted 5 June 2017; published online 16 June 2017)

We report the effect of different surface treatment and passivation techniques on the stability of InGaAs/InP heterojunction phototransistors (HPTs). An $In_{0.53}Ga_{0.47}As$ surface passivated with aqueous ammonium sulfide ($(NH_4)_2S$), aluminum oxide (Al_2O_3) grown by atomic layer deposition (ALD), and their combination is evaluated by using Raman spectroscopy and X-ray photoelectron spectroscopy (XPS). All samples were kept in the air ambient, and their performances were periodically measured to investigate their long-term stability. Raman spectroscopy revealed that the peak intensity of the GaAs-like longitudinal optical phonon of all passivated samples is decreased compared with that of the control sample. This is attributable to the diminution of the carriers near the passivated surfaces, which was proven by extracted surface potential (V_s). The V_s of all passivated samples was decreased to less than half of that for the control sample. XPS evaluation of As3d spectra showed that arsenic oxides (As_2O_3 and As_2O_5) on the surfaces of the samples can be removed by passivation. However, both Raman and XPS spectra show that the $(NH_4)_2S$ passivated sample reverts back over time and will resemble the untreated control sample. When capped with ALD-grown Al_2O_3, passivated samples irrespective of the pretreatment show no degradation over the measured time of 4 weeks. Similar conclusions are made from our experimental measurement of the performance of differently passivated HPTs. The ALD-grown Al_2O_3 passivated devices show an improved optical gain at low optical powers and long-term stability. *Published by AIP Publishing.*
[http://dx.doi.org/10.1063/1.4986633]

INTRODUCTION

$In_{0.53}Ga_{0.47}As$, which is lattice-matched to InP, has been extensively studied as a photo-absorption material of short wavelength infrared (SWIR) photodetectors for applications such as optical communication, night vision, astronomical telescopes, quantum cryptography, and nano-bio sensor systems.[1–6] Because the sensitivity of SWIR photodetectors could be a bottleneck in the overall system performance in these fields, efforts to enhance the signal-to-noise ratio (SNR) of the photodetectors at ultra-low optical power are essential. PIN photodiodes (PIN-PDs) and avalanche photodiodes (APDs) have recently been used as photodetectors for optical communication and imaging systems. However, PIN-PDs have no internal optical gain and APDs may suffer from high operating voltage, excess noise from avalanche multiplication, and unstable gain caused by material inhomogeneity. Heterojunction phototransistors (HPTs) have demonstrated large current gain at low bias voltage and compatibility with heterojunction bipolar transistors (HBTs) in terms of their epitaxial structures and fabrication process, which are potentially advantageous for the above applications. Although nonlinear gain dependency on the incident optical power is also favorable to the mixing process in applications involving optoelectronic mixers,[7] InGaAs/InP HPTs suffer from the dramatic reduction of the optical gain at low optical power levels, which is closely associated with the exposed base-collector (b-c) junction of mesa-type devices.[8] The abruptly terminated mesa sidewalls with relatively narrow bandgap lead to band bending at the surface. Thus, the Fermi level pinning produced by native surface oxide and nonradiative recombination centers results in exacerbation of the performance and reliability for the HPTs.

Because surface passivation is crucial for both realizing high performance and preserving functionalities of the devices, many efforts on the different passivation techniques to overcome the surface leakage issues have been conducted. Sulfur passivation,[9] Zn diffusion,[8] dielectric passivation,[10] and polymer coating[11] have been successfully utilized to improve the performance of the InGaAs-based photodetectors. All these techniques effectively removed the conductive native oxides and passivated the dangling bonds at the exposed InGaAs surface. Since $In_xGa_{1-x}As$ has shown great promise as a channel material for metal oxide semiconductor field effect transistors (MOSFETs), an atomic layer deposition (ALD)-grown aluminum oxide (Al_2O_3) film has been vigorously studied to achieve the good quality of oxide/InGaAs interfaces with a low interface state density.[12–14] While the thickness of the film can be precisely controlled on an atomic scale, Al_2O_3 has lower Gibbs free energy compared to that of the native oxides formed on InGaAs.[15] Formation reaction of Al_2O_3 thermodynamically takes precedence over the V oxide species, providing the clean starting surface of InGaAs prior to the deposition of the film which is known as the self-cleaning process.[16,17] Until now, ALD-grown Al_2O_3 seems to satisfy the most prominent passivation layer to enable unpinning of the Fermi level on the surface of the InGaAs. Nevertheless, very little research has been conducted on InGaAs/InP HPTs and other InGaAs-based optoelectronic

devices. Not only the capability of the surface passivation, but also its long-term reliability is very important. Surface aging evaluations are also needed to find out a truly viable approach.

In this work, we have selected aqueous ammonium sulfide ($(NH_4)_2S$) and ALD-grown Al_2O_3 for investigating the passivation and aging of the $In_{0.53}Ga_{0.47}As$ surface and optical performance of InGaAs/InP HPTs. Prior to the passivation process of the ALD-grown Al_2O_3, chemical treatments with and without $(NH_4)_2S$ were carried out. Raman spectroscopy and X-ray photoelectron spectroscopy (XPS) were utilized to analyze the changes in the surface chemistry over time for each passivation technique. Their reliability was also investigated through the measured characteristics of each passivated device.

EXPERIMENT

The epitaxial layers for the HPTs were grown by using a low-pressure metalorganic chemical vapor deposition (LP-MOCVD) system on a 3-in. (001) oriented sulfur doped InP substrate. Each HPT consists of a 500-nm-thick n^+-doped ($1 \times 10^{19}\,cm^{-3}$) InP buffer layer, a 25-nm-thick n^--doped ($5 \times 10^{15}\,cm^{-3}$) InGaAsP compositional graded layer, an 1.5-μm-thick n^--doped ($1 \times 10^{17}\,cm^{-3}$) InGaAs collector layer, a 100-nm-thick p^--doped ($2 \times 10^{17}\,cm^{-3}$) InGaAs base layer, a 25-nm-thick undoped InGaAsP spacer layer, a 200-nm-thick n^--doped ($1 \times 10^{16}\,cm^{-3}$) InP emitter layer, a 50-nm-thick n^--doped ($1 \times 10^{16}\,cm^{-3}$) InGaAsP step graded layer, and a 300-nm-thick n^+-doped ($1 \times 10^{19}\,cm^{-3}$) InGaAs cap layer. Zinc and Silicon are used for p-type and n-type dopants, respectively. The undoped quaternary layer on the base layer is utilized as the ledge structure for surface passivation. The other quaternary layers are for improving the carrier transport. Device fabrication begins with the definition of a 10-μm-diameter-emitter electrode of the HPTs. Non-alloyed Ti/Pt/Au (20/30/150 nm) metallization was evaporated and lifted-off for the emitter contact. The InGaAs cap layer, the InGaAsP step graded layer, and the InP emitter layer were etched with solutions of H_3PO_4:H_2O_2:H_2O, H_2SO_4:H_2O_2:H_2O, and H_3PO_4:HCl, respectively. The InGaAsP layers were left on the extrinsic base for passivation of the surface. The area of the optical window mesa is 30 $\times$ 30 μm^2, which defines an area of base-collector (B-C) junction. A 200-nm-thick SiN_x film was deposited by plasma-enhanced chemical vapor deposition (PECVD) at 300 °C for both anti-reflection (AR) coating and etch mask. Mesa isolation etching was performed from the SiN_x film down to the InGaAs collector layer by utilizing dry (CF_4) and wet (H_3PO_4-based solution) etches, followed by the CF_4-based dry etching for the opening in the SiN_x film on the emitter contact with a photoresist mask. Finally, the different passivation techniques were applied at the exposed B-C junction perimeter and InGaAs mesa sidewall. To investigate the effects of various surface treatments on the exposed $In_{0.53}Ga_{0.47}As$ surface, around 1-μm-thick undoped InGaAs collector layer in the device structure was prepared by utilizing the same etching processes of the device fabrication. Prior to each passivation process, all samples were cleaned with 10%NH_4OH solution for 2 min at room temperature. For the $(NH_4)_2S$ surface treatment for device A and sample A, they were dipped in aqueous 10%$(NH_4)_2S$ for 10 min at room temperature.[18] For the Al_2O_3-based surface passivation for device B and sample B, a 10-nm-thickness-Al_2O_3 was deposited at a temperature of 250 °C by using a thermal ALD system (Savannah S100) using alternating pulses of a trimethylaluminum (TMA) precursor and H_2O oxidant. Device C and sample C received the same $(NH_4)_2S$ treatment and ALD-grown Al_2O_3 step by step. A schematic diagram of the fabricated devices and samples is illustrated in Fig. 1, respectively. The control refers to the device and sample without any surface treatments. After the passivation, all the devices and samples were stored at indoor ambience. Measurements were taken immediately after performing the different treatments and then each week.

Raman spectroscopy was performed using a Jobin–Yvon Horiba LabRam HR Evolution spectrometer, equipped with a high efficiency thermal cooled CCD detector, a confocal microscope (Olympus), a holographic notch filter, and 1800 grooves/mm grating. Raman spectra were measured in the backscattering configuration at room temperature using a

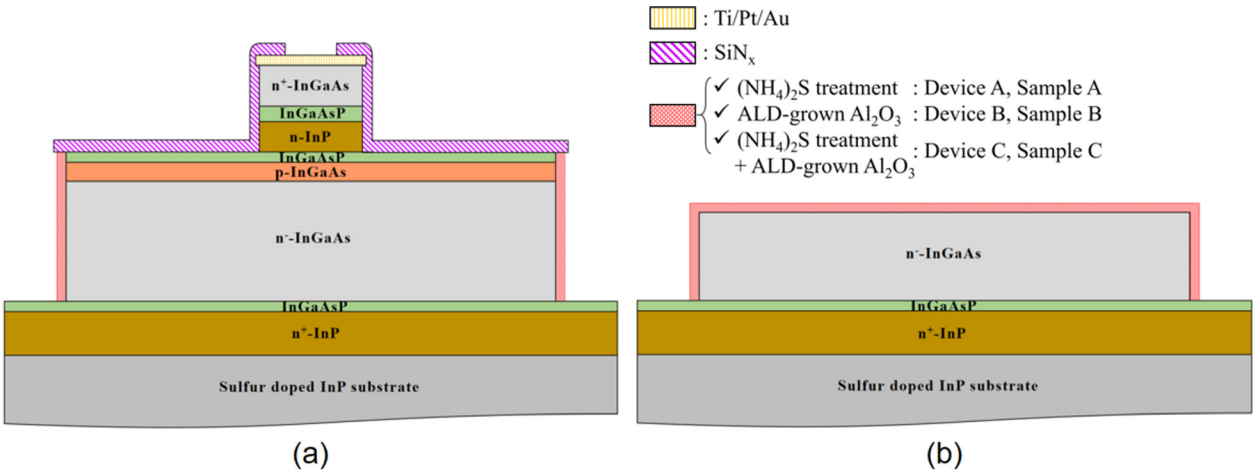

FIG. 1. Schematics of (a) the fabricated InP/InGaAs HPTs and (b) the studied Samples A, B, and C with different passivation techniques on the surfaces of the n^--InGaAs collector.

50× objective focusing the 532 nm line as an exciting source. An appropriate neutral density filter was used such that the power at the sample was kept at a maximum of 2.5 mW to minimize the photoexcitation effect.[19] The Raman spectrum was collected with repeated 5 accumulations at each of 10 s. Data acquisition and baseline correction were carried out with the commercially available software program LabSpec 6 (HORIBA Scientific). XPS measurements were performed in a commercial spectrometer (Thermo Scientific ESCALAB 250Xi) with a monochromatic Al Kα (1486.74 eV) X-ray source and care taken to avoid exposure to visible light. The pressure in the vacuum chamber during the analysis was less than 10^{-9} bar. Each scan was recorded as the average of five sequential scans. All the binding energies were referenced to the adsorbed carbon C1s peak, which was set to 284.8 eV. Fitting was performed via an automated routine implemented in MATLAB wherein the bands were fit to a sum of Gaussian peaks plus a linear background.

The electrical and optical performances of the fabricated HPTs were characterized by utilizing a 1.55-μm laser source (AQ4321A) and a multimeter (34410A) connected with a low-noise current preamplifier (SR 570) at room temperature. The light signal was delivered to the devices by a 50× objective lens. For laser power calibration, the incident optical power through the objective lens was measured using a commercial InGaAs-based PIN-PD module in a dark condition.

RESULTS AND DISCUSSION

A comparison of the normalized Raman scattering spectra of the $In_{0.53}Ga_{0.46}As$ samples for the different surface treatments is shown in Fig. 2(a). It is commonly observed that disorder-activated longitudinal acoustic (DALA) phonon of $In_xGa_{1-x}As$ having the mid-range of composition resides in the broad Raman band from 100 to 190 cm^{-1}.[20] Although the mode frequency and relative intensity are dependent on the composition and the doping concentration of material, the measured Raman result of the control sample displays InAs-like and GaAs-like longitudinal optical (LO) phonon modes located at 227 and 258 cm^{-1}, respectively. Coupled LO phonon-plasmon modes (L^- and L^+) originated from the free carriers in the bulk and the unscreened LO phonon emitted from the surface depletion layer combine to form the GaAs-like LO mode typically in the doped $In_{0.53}Ga_{0.47}As$.[21–23] The higher frequency band having a peak intensity at around 486 cm^{-1} is the coupled mode L^+, as shown in the inset of Fig. 2(a), which is associated with the doping concentration and is in good agreement with the theoretical value of a doping level of 5×10^{17} cm^{-3}.[22] After the NH_4OH cleaning of the surface, there are no remarkable changes in the Raman spectrum compared to the control sample. While the NH_4OH treatment is well known for removing arsenic and gallium native oxides from the surface,[24] it is believed that the hydroxylated cleaning is not sufficient to cause a detectable change of the surface state based on the Raman spectrum. While the position of the InAs-like LO mode remains unchanged, however, the GaAs-like LO mode slightly shifts to lower frequency from 258 to 255 cm^{-1} in samples A, B, and C. We also found that their peak intensities in the GaAs-like LO mode and the coupled L^+ mode are decreased compared with that of the control sample. These changes might be attributed to the diminution of the free carriers due to the surface passivation.[25,26] Accordingly, the depletion layer thickness at the surface is decreased so that the intensity of the GaAs LO-mode is diminished. After aging the passivated samples, the Raman spectra are measured under the same experimental condition as shown in Fig. 2(b). We observed that there is no perceptible change in the Raman spectra with time from the control sample (not shown). Samples B and C exhibit little change in the Raman results, indicating that their surface states are almost unchanged. However, the GaAs LO-mode and coupled L^+ mode of sample A with time turn into those measured from the surface of the control sample. We believe that the carrier accumulation begins at the $(NH_4)_2S$ passivated surface over time. Therefore, it induces the surface band bending of which curvature can be determined from the surface potential.

To quantify the variations of the surface potential for each sample, the Raman spectra, which are in the frequency range of the InAs-like and GaAs-like LO modes for the control sample, determined by nonlinear least squares fitting are given in Fig. 3(a). The disaggregated five peaks exhibit TO-InAs, LO-InAs, TO-GaAs, L^-, and LO-GaAs located at 208, 227, 242, 255, and 266 cm^{-1}, respectively. While the peak frequencies are set constant, the spectra of all passivated samples are extracted by the peak fitting procedure. Figure 3(b) shows the fitting curves to Raman data of the representative passivated sample B. It clearly appears that

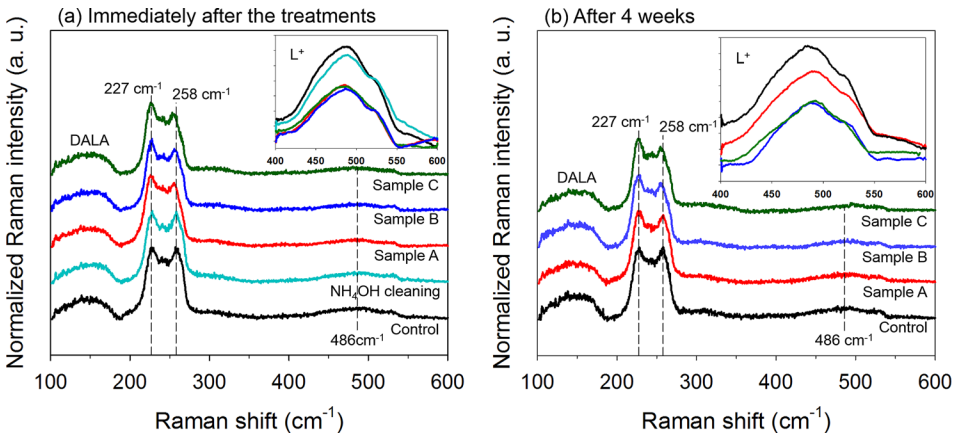

FIG. 2. Normalized Raman scattering spectra of the $In_{0.53}Ga_{0.47}As$ collector layer for the different treatments measured (a) immediately after the treatment and (b) after aging for 4 weeks. Both insets show each L^+ Raman band enlarged from 400 to 600 cm^{-1} and they are filtered with the smoothing method (moving average) to clarify the comparison.

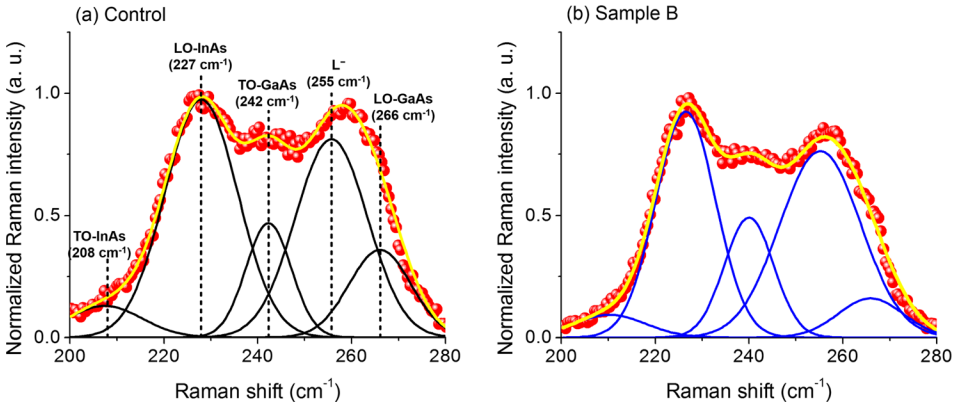

FIG. 3. Details of the peak fitting to (a) the control and (b) sample B of the same Raman spectra as in Fig. 2(a). Two spectra are found by nonlinear least squares fitting to five peaks centered at 208 cm^{-1} (L*), 227 cm^{-1} (LO-InAs), 242 cm^{-1} (R), 255 cm^{-1} (L^-), and 266 cm^{-1} (LO-GaAs).

the intensity of the LO-GaAs phonon included in the tail of the L^- peak is weaker than that of the control sample. The same result could be observed in Sample A and Sample C. The surface potential V_s can be estimated from ratio R between the measured intensity of the LO-GaAs mode and L^- peak. When R_0 is defined as the ratio between the intensity of the LO-GaAs mode of the undoped material and L^- peak if there were no depletion layer, the R is described by[25]

$$R = R_0 \frac{(1 - e^{-2w/\delta})}{e^{-2w/\delta}},$$

where δ is the penetration depth of the excitation wavelength and w is the depletion depth from the surface. The calculated δ of $In_{0.47}Ga_{0.53}As$ at 532 nm of the excitation wavelength is around 41 nm at room temperature. The w is defined by $w = \sqrt{2\varepsilon V_s/qn}$, where ε is the permittivity of the material and n is the doping concentration. Therefore, the relation of the V_s with the experimental R value can be given by[26]

$$V_s = \frac{qn}{2\varepsilon}\left[\frac{\delta}{2}\ln\left(1 + \frac{R}{R_0}\right)\right]^2.$$

The R_0 value can be determined if the $V_s = 0.4$ V is assumed for the control sample. Therefore, it is possible to evaluate the V_s for the all passivated samples. The detailed parameters including R, w, and V_s of each type of the sample are listed in Table I. The parameters are obtained by averaging over 5 different locations of each sample. The average V_s values of samples A, B, and C decrease to less than half that of the control sample. These results demonstrate convincingly that sample A only exhibits the increased V_s after the aging while the V_s of the others is almost kept constant. Besides, the V_s is rarely changed after the NH_4OH cleaning. Figure 4(a) shows the energy band diagram for the free surface of n-InGaAs. Negatively charged surface states repel free electrons from the surface, thereby leading to the depletion layer, w, with the V_s to conserve the charge neutrality. On the other hand, the energy band diagram of the Al_2O_3/n-InGaAs interface can be anticipated as shown in Fig. 4(b). The ALD-grown Al_2O_3 passivation (Samples B and C) results in the decreased density of the surface states so that the w is decreased.

TABLE I. Comparison of the surface properties of the all passivated samples in the initial state and after aging for 4 weeks. Assuming that $V_s = 0.40$ V for the control sample, the R_0 of 0.10 was obtained.

		R	w (nm)	V_s (V)
Control		0.44	35.06	0.40
NH_4OH cleaning		0.42 ± 0.03	34.25 ± 0.19	0.38 ± 0.03
Sample A	Initial state	0.20 ± 0.03	22.82 ± 0.17	0.17 ± 0.03
	After 4 weeks	0.32 ± 0.05	29.72 ± 0.25	0.28 ± 0.05
Sample B	Initial state	0.21 ± 0.02	23.56 ± 0.13	0.18 ± 0.02
	After 4 weeks	0.21 ± 0.01	23.59 ± 0.07	0.18 ± 0.01
Sample C	Initial state	0.19 ± 0.02	22.17 ± 0.14	0.16 ± 0.02
	After 4 weeks	0.20 ± 0.03	22.82 ± 0.21	0.17 ± 0.03

Obviously, the increased V_s is associated with chemistry at the surface of the $In_{0.53}Ga_{0.47}As$. It is considered that the main deleterious influence to induce the band bending is due to the volatile V oxide species.[27] The normalized As3d XPS spectrum of the $In_{0.53}Ga_{0.47}As$ surface is exemplified in the control sample as shown in Fig. 5(a). The peaks of the bulk In-Ga-As, elemental As-As, As_2O_3, and As_2O_5 are found by the Gaussian fitting method. The observed native arsenic oxides, As_2O_3 and As_2O_5, result in the surface leakage channels at the etched plane of the $In_{0.53}Ga_{0.47}As$.[28] Although the intensity came from the arsenic oxides after the NH_4OH cleaning is decreased compared with the control sample, the native oxides still existed as shown in Fig. 5(b). We have estimated that the little change of the obtained V_s from the Raman spectrum for the NH_4OH-cleaned sample goes along with the XPS analysis. It is likely difficult to totally remove the As_2O_3 rather than As_2O_5 with NH_4OH cleaning, indicating that the As_2O_3 has a higher Gibb free energy than the As_2O_5.[15]

A comparison of the XPS As3d spectra for the passivated interfaces/InGaAs measured immediately after the treatments is shown in Fig. 6(a). All passivated samples display that there are no observable residues of the arsenic oxides. However, Fig. 6(b) shows that the samples began to implicate the different variance in the As3d spectra after aging for 4 weeks. The arsenic oxides were recreated on the surface of sample A and their signal intensity tends to increase with time, as shown in the inset of Fig. 6(b). The effect of the $(NH_4)_2S$ treatment for the $In_{0.53}Ga_{0.47}As$ fades during exposure to air so that the recreated oxides might deteriorate the surface properties. The increased signal intensity was finally comparable with the intensity of the control sample at the 4th week. Samples B and C exhibit that there are no detectable changes in the As3d spectra after the aging period,

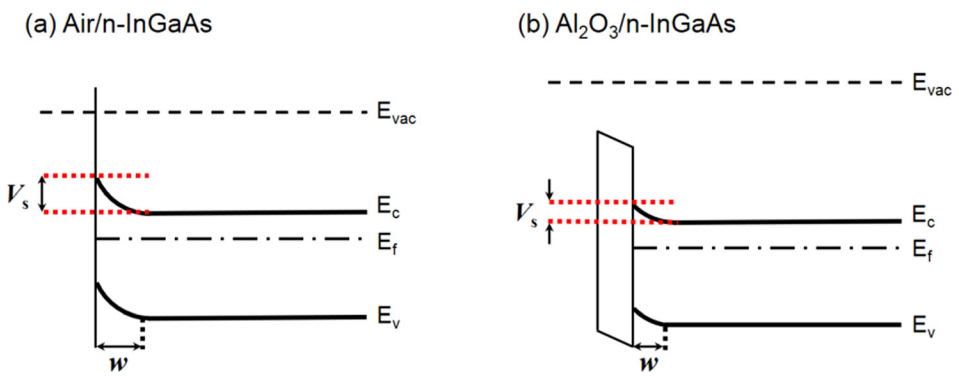

FIG. 4. Schematic energy band diagram of (a) air/n-InGaAs and (b) Al_2O_3/n-InGaAs interfaces.

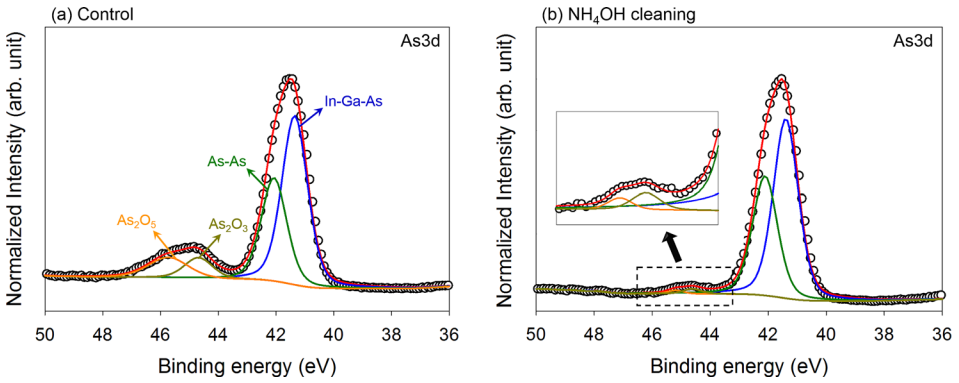

FIG. 5. Peak fitted As3d in XPS spectra for the $In_{0.53}Ga_{0.47}As$ surface (a) of the control and (b) after the NH_4OH cleaning. The inset shows the enlarged As3d spectra of the arsenic oxides.

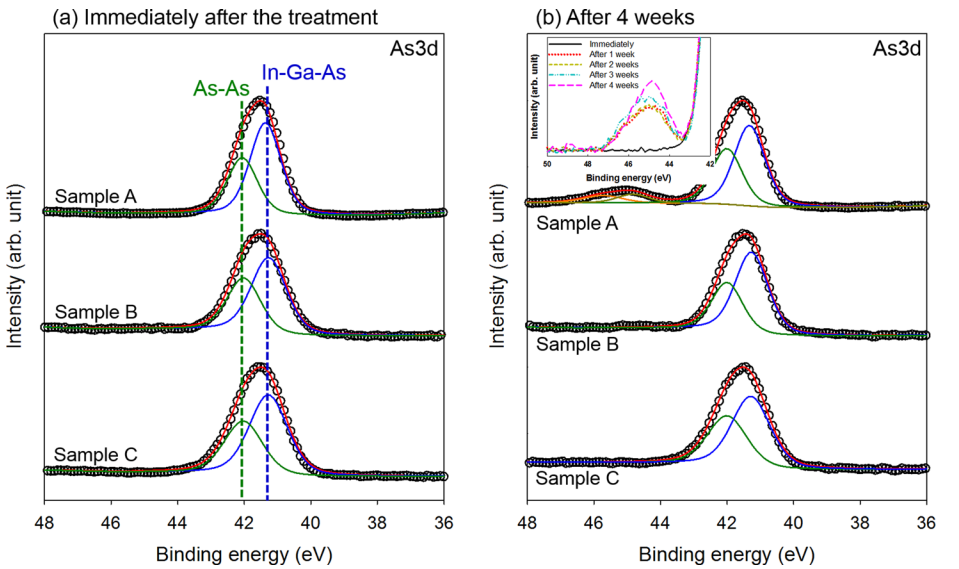

FIG. 6. Peak fitted As3d in XPS spectra for the $In_{0.53}Ga_{0.47}As$ surface of samples A, B, and C (a) immediately after the treatment and (b) after aging for 4 weeks. The inset shows the enlarged As3d spectra of the arsenic oxides of sample A with time.

irrespective of the pretreatments before the Al_2O_3 growth. Although it hardly gets rid of the arsenic oxides with the NH_4OH cleaning, the interface quality of sample B is analogous to sample C after the Al_2O_3-grown ALD process, indicating that the interfacial self-cleaning effect is shown to sample B.

The respective surface passivation techniques were applied to the HPTs and their optical performances were characterized. To make the comparison more reliable, at least 10 devices from each passivation method were measured. Figure 7(a) shows the mean values of collector dark current (I_D) as a function of collector-emitter voltage (V_{CE}) for each device at room temperature. The measured collector dark currents (I_Ds) of the control device, device A, device B, and device C at $V_{CE} = 1$ V are 3.1, 3.0, 6.0, and 5.7 nA, respectively. No noticeable differences are observed in the I_Ds for the both control device and device A because we have believed that the surface state of the fresh control device might be similar to that of the device A. The I_Ds of device B and C are fairly comparable but larger than that of the control device. The increased I_D in the both devices is attributed to the increased optical gain. Electron-hole pairs are generated in the collector region where the incident photons are absorbed and the electrons and holes are separated by a built-in field and an externally applied bias field. The holes move toward the base region and are accumulated in the base layer within the recombination time. The accumulated holes in the base layer change the quasi-Fermi level for holes, which

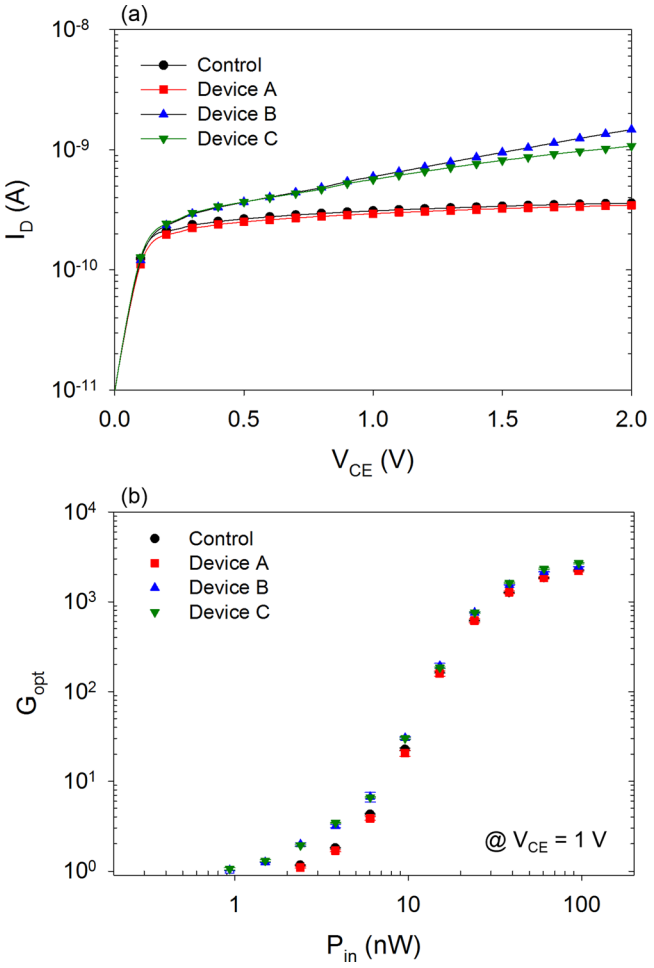

FIG. 7. (a) Collector dark current as a function of collector-emitter bias voltage and (b) optical gain at $V_{CE} = 1.0$ V with respect to incident optical powers for the different passivated devices.

results in a reduction of the potential barrier for electrons injected from the emitter. The electrons finally injected from the emitter to the collector, resulting in total photocurrent with optical gain. Here, the amount of downshift in the quasi-Fermi level of holes depends on the density of holes in the intrinsic base. During the transport of holes through the collector and the extrinsic base, some holes are captured by the surface states and hence the optical gain is decreased. Those holes are protected from the annihilation by passivating with the ALD-grown Al_2O_3 at the exposed collector sidewall and the base-collector junction. The measured I_D is the external dark current, which can be obtained by multiplying the internal dark current by the optical gain.[29,30] Therefore, the increased optical gain caused by the passivation results in the increased I_D. The optical gain of HPTs is defined as $G_{opt} = h\nu\Delta I_c/qP_{in}$, where $h\nu$ is the energy of an incident photon and ΔI_c is the difference between collector photocurrent (I_P) and I_D. Figure 7(b) shows a comparison of the G_{opt} with standard error for each device according to optical power levels from 0.9 to 95.8 nW at a wavelength of 1.55 μm. It obviously denotes that devices B and C exhibit a higher G_{opt} than the control device over the investigated range of the P_{in} and their light detection limits to as low as 1 nW of the P_{in}. However, the G_{opt} of the control device and device A barely exceeds unit gain at 2.4 nW of the P_{in}. Therefore, the external dark current of devices B and C divided by the G_{opt} at $V_{CE} = 1.0$ V and $P_{in} = 2.4$ nW is exactly the same as the internal dark current of the control device under the same condition. The $(NH_4)_2S$ treatment even seems to slightly degrade the G_{opt} of the HPTs compared to the fresh control device. Although the $(NH_4)_2S$ treatment removed the native oxides on the InGaAs in the initial state in accordance with the Raman and XPS results, the enhanced optical performance in device A could not be expected. Since some works on deterioration of optical performances of III-V material based photodetectors after Sulphur passivation has been reported,[31,32] optimum conditions for the passivation such as duration time, coating method, temperature, and concentration might be necessary to circumvent an unexpected result.

For the comparative study on the stable passivation method, aging testing of each device for periods up to 4 weeks in the atmosphere was conducted. The I_D shift at $V_{CE} = 1.0$ V for each type of the HPT device is shown in Fig. 8(a). The average I_D shifts from the initial state to 4 weeks were +1.6 and +0.5 nA for the control device and device A, respectively. Both devices showed that the I_D value is gradually increased as time passes. One can assume that the exposed InGaAs surfaces in the control device are oxidized and hence worsen the device performance. Furthermore, the increased I_D in device A is closely related to a progressive loss of Sulphur atoms

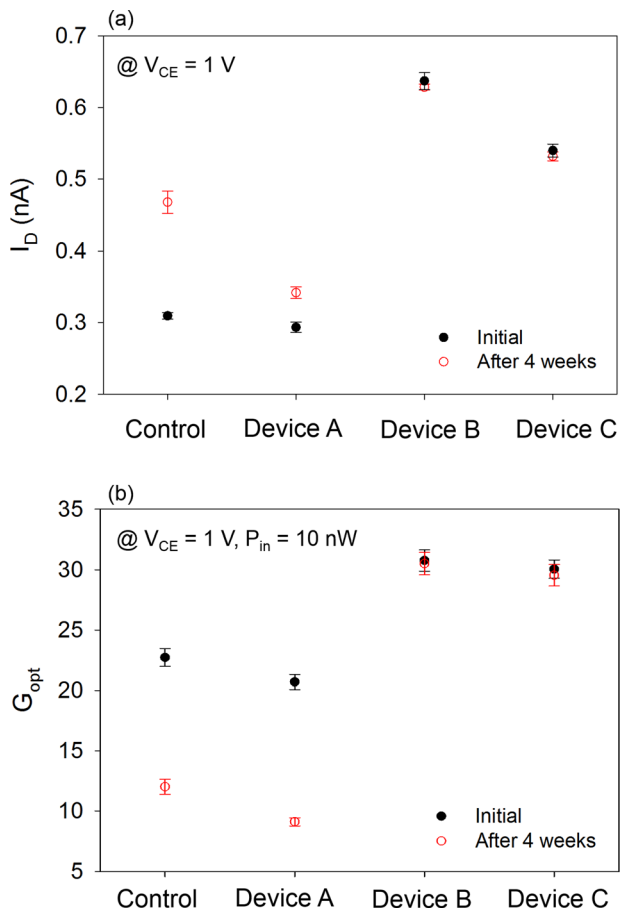

FIG. 8. (a) Collector dark current at $V_{CE} = 1.0$ V and (b) optical gain at $V_{CE} = 1.0$ V and $P_{in} = 9.6$ nW for the individual passivated devices in the initial state and after aging for 4 weeks.

from the surface. On the other hand, there are no remarkable shifts in the I_D values of devices B and C. In addition to the I_D, the variation of the G_{opt} at $V_{CE} = 1.0$ V and $P_{in} = 9.6$ nW for each type of devices is shown in Fig. 8(b). The average G_{opt} of 22.7 and 20.7 for the control device and device A decreases to 47.1% and 56.0% after 4 weeks, respectively. Consequently, the increased external dark current in the control device or device A is attributed to the decline in the device performance, not to the increased G_{opt}. Devices B and C showed a stable G_{opt} with the flight of time, indicating that the $In_{0.53}Ga_{0.47}As$ surface has been protecting and retaining by the ALD-grown Al_2O_3 film in the ambient condition. Since 4 weeks, the control device and device A have shown to saturate the decreased G_{opt} while devices B and C have been preserving their G_{opt} much over several months.

CONCLUSION

Comparative studies of surface passivation and aging with the aqueous $(NH_4)_2S$ or/and ALD-grown Al_2O_3 applied to the $In_{0.53}Ga_{0.47}As$ layer and InGaAs/InP HPTs were undertaken. The surface stability and interface quality over time for the separate passivated samples were investigated by Raman spectroscopy and XPS. We observed that the peak intensities of the GaAs-LO mode and coupled L^+ mode of all passivated samples are relatively decreased due to the diminution of the carriers at the passivated surfaces. The V_s extracted from the Raman spectra justified that the ALD-grown Al_2O_3 on the $In_{0.53}Ga_{0.47}As$ (sample B and C) regardless of the pretreatment is superior passivation compared to the $(NH_4)_2S$ (sample A). The XPS As3d spectra also proved that the arsenic oxides (As_2O_3 and As_2O_5) totally removed from the $(NH_4)_2S$ passivation at the initial stage are reproduced over time, while there are no detectable signals from the arsenic oxides in the ALD-grown Al_2O_3 passivated samples after the aging period. Moreover, we found a similar conclusion in the optical performances of the different passivated HPTs. The G_{opt} of the ALD-grown Al_2O_3 passivated HPTs irrespective of the pretreatment was enhanced at the low optical power levels compared to the control and the $(NH_4)_2S$ passivated devices. The good durability of I_D and G_{opt} over time is also shown in the ALD-grown Al_2O_3 passivated HPTs. The experimental results would invite expectation that the ALD-grown Al_2O_3 is promising for a long-term passivation technique for the InGaAs/InP HPTs capable of detecting ultra-low optical power.

ACKNOWLEDGMENTS

This work made use of the Keck-II facility of Northwestern University's NUANCE Center, which has received support from the Soft and Hybrid Nanotechnology Experimental (SHyNE) Resource (NSF ECCS-1542205); the MRSEC program (NSF DMR-1121262) at the Materials Research Center; the International Institute for Nanotechnology (IIN); the Keck Foundation; and the State of Illinois, through the IIN.

[1]J. B. D. Soole and H. Schumacher, IEEE J. Quantum Electron. **27**, 737 (1991).
[2]D. C. Dayton, J. Allen, R. Nolasco, J. D. Gonglewski, M. Myers, D. Burns, I. Mons, and F. Maia, Proc. SPIE **8014**, 801407 (2011).
[3]M. Rezaei, M. S. Park, S. Wheaton, C. L. Tan, V. Fathipour, O. Guyon, M. P. Ulmer, and H. Mohseni, Proc. SPIE **9915**, 99150P (2016).
[4]O. G. Memis, A. Katsnelson, S. Kong, H. Mohseni, M. Yan, S. Zhang, T. Hossain, N. Jin, and I. Adesida, Appl. Phys. Lett. **91**, 171112 (2007).
[5]N. Gisin, G. Ribordy, W. Tittel, and H. Zbinden, Rev. Mod. Phys. **74**, 145 (2002).
[6]S. W. Chu, I. H. Chen, T. M. Liu, C. K. Sun, S. P. Lee, B. L. Lin, P. C. Cheng, M. X. Kuo, D. J. Lin, and H. L. Liu, J. Microsc. **208**, 190 (2002).
[7]C. P. Liu, A. J. Seeds, and D. Wake, IEEE Microwave Guided Wave Lett. **7**, 72 (1997).
[8]S. W. Choi, S. Furue, N. Hayama, K. Nishida, and M. Ogura, IEEE Photonics Technol. Lett. **21**, 1187 (2009).
[9]M. R. Ravi, A. DasGupta, and N. DasGupta, IEEE Trans. Electron Devices **50**, 532 (2003).
[10]Y. Zhou, X. Ji, M. Shi, H. Tang, X. Shao, X. Li, H. Gong, X. Cao, and F. Yan, J. Appl. Phys. **118**, 034507 (2015).
[11]I. Watanabe, M. Tsuji, M. Hayashi, K. Makita, and K. Taguchi, IEEE Photonics Technol. Lett. **8**, 824 (1996).
[12]P. D. Ye, G. D. Wilk, B. Yang, J. Kwo, H.-J. L. Gossmann, M. Hong, K. K. Ng, and J. Bude, Appl. Phys. Lett. **84**, 434 (2004).
[13]M. Yokoyama, R. Iida, S. Kim, N. Taoka, Y. Urabe, H. Takagi, T. Yasuda, H. Yamada, N. Fukuhara, M. Hata, M. Sugiyama, Y. Nakano, M. Takenaka, and S. Takagi, IEEE Electron Device Lett. **32**, 1218 (2011).
[14]M. H. Lin, Y. C. Lin, Y. S. Lin, W. J. Sun, S. H. Chen, Y. C. Chiu, C. H. Cheng, and C. Y. Chang, ECS J. Solid State Sci. Technol. **6**, Q58 (2017).
[15]G. Hollinger, R. Skheyta-Kabbani, and M. Gendry, Phys. Rev. B **49**, 11159 (1994).
[16]C. H. Hou, M. C. Chen, C. H. Chang, T. B. Wu, C. D. Chiang, and J. J. Luo, J. Electrochem. Soc. **155**, G180 (2008).
[17]M. Milojevic, F. S. Aguirre-Tostado, C. L. Hinkle, H. C. Kim, E. M. Vogel, J. Kim, and R. M. Wallace, Appl. Phys. Lett. **93**, 202902 (2008).
[18]É. O'Connor, B. Brennan, V. Djara, K. Cherkaoui, S. Monaghan, S. B. Newcomb, R. Contreras, M. Milojevic, G. Hughes, M. E. Pemble, R. M. Wallace, and P. K. Hurley, J. Appl. Phys. **109**, 024101 (2011).
[19]F. Schäffler and G. Abstreiter, Phys. Rev. B **34**, 4017 (1986).
[20]H. Kawamura, R. Tsu, and L. Esaki, Phys. Rev. Lett. **29**, 1397 (1972).
[21]K. Kakimoto and T. Katoda, Appl. Phys. Lett. **40**, 826 (1982).
[22]T. P. Pearsall, R. Carles, and J. C. Portal, Appl. Phys. Lett. **42**, 436 (1983).
[23]N. Matrullo, M. Constant, G. Sagon, R. Fauquembergue, and A. Leroy, J. Raman Spectrosc. **26**, 167 (1995).
[24]B. Brennan, M. Milojevic, R. Contreras-Guerrero, H. C. Kim, M. Lopez-Lopez, J. Kim, and R. M. Wallace, J. Vac. Sci. Technol. B **30**, 04E104 (2012).
[25]L. A. Farrow, C. J. Sandroff, and M. C. Tamargo, Appl. Phys. Lett. **51**, 1931 (1987).
[26]B. Boudart, C. Gaquière, S. Trassaert, M. Constant, A. Lorriaux, and N. Lefebvre, Appl. Phys. Lett. **74**, 3221 (1999).
[27]H. J. Oh, S. A. B. Suleiman, and S. Lee, J. Electrochem. Soc. **157**, H1051 (2010).
[28]O. Salihoglu, J. Vac. Sci. Technol. B **32**, 051201 (2014).
[29]V. Fathipour, O. G. Memis, S. J. Jang, R. L. Brown, I. H. Nia, and H. Mohseni, IEEE J. Sel. Top. Quantum Electron. **20**, 3805106 (2014).
[30]M. Rezaei, M. S. Park, C. L. Tan, and H. Mohseni, "Sensitivity limit of nanoscale phototransistors," preprint arXiv:1704.05987 (2017).
[31]J. Hoffmann, T. Lehnert, D. Hoffmann, and H. Fouckhardt, Semicond. Sci. Technol. **24**, 065008 (2009).
[32]D. Sheela and N. DasGupta, in *IEEE International Conference on Indium Phosphide & Related Materials, Newport Beach, CA* (2009), p. 274.